A holistic approach towards revisiting cathode-electrolyte interfaces in battery systems

Jie Xiao[*1,2], Nicole Adelstein[3], Yujing Bi[1], Wenjuan Bian[4], Jordi Cabana[5], Corie Cobb[2], Yi Cui[6,7], Shen Dillon[8], Marca Doeff[9], Saiful Islam[10], Kevin Leung[11], Mengya Li[12], Feng Lin[13], Jun Liu[1,2], Hongmei Luo[14], Amy Marschilok[15,16], Ying Shirley Meng[17], Yue Qi[18], Ritu Sahore[12], Kayla Sprenger[19], Robert Tenent[20], Michael Toney[19], Wei Tong[8], Liwen Wan[21], Chongmin Wang[1], Bingbin Wu[1], Yaobin Xu[1],

[1]Pacific Northwest National Laboratory, Richland, WA, United States
[2]University of Washington, Seattle, WA, United States
[3]San Francisco State University, San Francisco, CA, United States
[4]Idaho National laboratory, Idaho Falls, ID, United States
[5]Argonne National Laboratory, Lemont, IL, United States
[6]SLAC National Accelerator Laboratory, Menlo Park, CA, United States
[7]Stanford University, Stanford, CA, United States
[8]University of California Irvine, CA, United States
[9]Lawrence Berkeley National Laboratory, Berkeley, CA, United States
[10]Jackson State University, Jackson, MS, United States
[11]Sandia National Laboratories, Albuquerque, NM, United States
[12]Oak Ridge National Laboratory, Oak Ridge, TN, United States
[13]Virginia Tech, Blacksburg, VA, United States
[14]New Mexico State University, Las Cruces, NM, United States
[15]Brookhaven National Laboratory, United States
[16]Stony Brook University, Stony Brook, NY, United States
[17]University of California San Diego, CA, United States
[18]Brown University, Providence, RI, United States
[19]University of Colorado Boulder, Boulder, CO, United States
[20]National Renewable Energy Laboratory, Golden, CO, United States
[21]Lawrence Livermore National Laboratory, Livermore, CA, United States

Corresponding author. Email: jie.xiao@pnnl.gov

Almost all electrode couples in electrochemical cells operate beyond the thermodynamic stability limits of the electrolytes[1]. In many cases, these cells only operate because the reactions between electrode and electrolyte result in the formation of new phases (or interphases) at the electrode–electrolyte interfaces. For example, the stable solid electrolyte interphase (SEI) layer[2] formed on graphite surfaces has enabled the commercialization of Li-ion batteries. Although some similarities can be found between good SEI and cathode-electrolyte interface (CEI) layers in terms of stability, dense structures, low impedance, thickness, etc, the desired attributes of CEI depend on the specific cathodes and battery systems. There is no universal CEI (or SEI) that can meet the expectations of all different applications. A thin CEI layer is usually preferred for fast ion diffusion,[3-5] while in other occasions a denser CEI helps mitigate dissolution challenges of transition metal cations.[6,7] A stable CEI at a high cutoff voltage, e.g., beyond 4.3 V (vs. Li/Li^+) helps extract more energy from traditional layered cathodes. For $LiFePO_4$-based chemistries designed for thousands of stable cycles, CEI layers are quite stable within the electrochemical stability window (up to 3.5 V) and therefore, durability and minimum impedance growth upon cycling become more important.

The CEI has not attracted as much attention as its SEI counterpart. The main reason is probably because as long as the cutoff voltage of the battery is not greater than 4.2 V, most of the carbonate-based electrolyte is quite stable on the cathode side but decomposes more aggressively on the anode driven by the electrochemical potentials. As the demand for high energy batteries continues to grow, in addition to the exploration of new high energy materials[8,9], it is equally important to increase the battery operation voltage appropriately so more capacity and energy can be extracted from the same cathode materials in the cell and pack, assuming that the cathode structure does not change much.

At elevated voltages, a stable CEI layer becomes critical for battery performances, in addition to the structural stability of cathode itself. Similar to the SEI, the CEI is generated through the decomposition of electrolytes but at high voltages. The CEI passivates cathode surfaces, [10] directly determines the reversibility of ion transport, and dictates the kinetics of the cathode and thus overall cell reactions, assuming the SEI or anode is not the limiting step. In addition to electrolyte recipes, cathode surface chemistry[11], morphologies[12], and electrochemical potential[13] all profoundly impact CEI components and properties.

Although there are already many publications on CEI, there is still not an unequivocal conclusion how to design and control these layers at the molecular level. Some of the potential reasons behind the inconsistent and sometimes controversial discoveries on CEI include but are not limited to:

(1) **Lack of model materials with controllable surface properties:** Many cathode materials used for CEI studies are synthesized in the lab, leading to variations in particle sizes, morphologies, and even stoichiometry.[14,15] The higher surface areas of smaller cathode particles intensify side reactions and impact CEI formation.[16-18] Even when commercial cathode materials (e.g., NMC811) are used, depending on th. storage conditions, the surface chemistry of NMC811 changes significantly particularly if exposed to air. [19] The drastically different surface and bulk properties of cathode materials very often determine the observed electrochemical performances, making it hard to isolate the CEI's effect in the electrochemical cell.

(2) **Reliable design of electrochemical cells for operando characterization:** Electrochemical cells designed for in situ characterization usually introduce a significant increase in cell

impedance because of their drastically downsized cell format. In the miniaturized cell, the increased relative distance between cathode and anode is another contributor to the high impedance, particularly because of the non-aqueous electrolyte. Rational design of *in situ* electrochemical cells is critical in determining if an observation is a common phenomenon in CEI or only exists in the given operando characterization test due to the design of the small-scale cells with high impedances.[20]

(3) **CEI derived from flooded electrolytes vs. CEI formed in lean electrolytes:** Most characterizations are conducted on materials in cells flooded with electrolyte that is often one order of magnitude more than what is practically used in real batteries[21]. The significantly higher amount of electrolyte in flooded cells facilitates CEI dissolution which reforms during cycling. Thus, CEI composition and thickness continuously change. These changes make the observed properties of CEI debatable when it comes to real batteries, in which the CEI is derived from very lean electrolyte.

(4) **Cell failure is NOT dominantly caused by CEI if the cathode is coupled with a poor anode:** The electrochemical performance of a cell is determined by the worst electrode including its interphase, assuming separators and electrolyte are reasonably good and not the limiting step that impedes Li^+ transport. For the initial assessment of CEI, half cells using lithium metal as the counter electrode will provide useful information on CEI especially in the early stage of electrochemical reactions. Upon cycling, however, the lithium metal anode itself becomes unstable. Cell impedance increases drastically, and dominates the cell instability. To fully understand the CEI and its evolution, especially after extensive cycling, a stable anode and its SEI are prerequisites. Full cells using stable graphite (and stable SEI) as the anode are necessary to ensure that the electrochemical reaction is mainly controlled by the CEI during extensive cycling to provide the accurate elaboration and understanding of the electrochemical data.

A full understanding of CEI formation and evolution at varied length and time scales, especially at high voltages, is still lacking but urgently needed to better tune CEI properties at the atomic scale to further stabilize the electrochemical energy storage system.

Revisiting CEI at relevant scales

Full coin cell protocols to ensure CEI dictates the performance: To understand and address CEI challenges at high voltages, one prerequisite is to ensure that the interfacial phenomena captured between cathode and electrolyte are also those happening in the practical batteries and dominate the electrochemical performance. This is because the performance of any electrochemical cell is dictated by the slowest step or worst component during battery operation.[22]If the observed electrochemical performance is not dominated by the CEI, it is challenging to assess if further modification of the cathode or CEI really helps because the cell performances do not reflect the CEI.

Correspondingly, a stable anode such as graphite is necessary to effectively evaluate CEI and cathode behaviors. If lithium metal is used as the counter electrode, there is always a sufficient source of Li^+ ions in the cell., whereas in cells with graphite anodes, the lithium inventory is restricted to that provided by the cathode. Therefore, the usable capacity of cathode during the initial cycling can be fully realized which is helpful to understand its materials properties. But the

long-time cycling of those Li metal-based cells mainly reflects lithium metal problems instead of cathode/CEI stability.[21] Unlike lithium metal half cells, graphite-based full coin cells have more parameters requiring control, from electrode coating to cell assembly and testing, to ensure reproducibility.[23] Table 1 lists the necessary parameters to construct and test full coin cells under conditions that are relevant to practical batteries. More details about the assembly process can be found in our previously published paper. [23]Depending on the intended application, the areal loading and porosity of cathode (and anode) in Table 1 can be further tuned for high energy, high power, or fast charging battery systems.

Note that coin cells using lithium metal anodes are still very helpful in assessing properties of electrode materials, including the initial capacities as discussed earlier, and are helpful for designing a balanced cell with appropriate N/P (negative/positive) ratios in the full cells. For characterization purposes, especially *in situ* or operando probing, coin cells using lithium metal anode simplifies the assembly process. The CEI formation during the initial cycling of those half cells will not become considerably different from that in graphite-based full coin cells. It is when the long-term stability of CEI becomes the focus of study that coupling with a stable graphite anode is necessary to ensure that the CEI dictates the cell performance.

As mentioned earlier, another issue of using a coin cell as the testing vehicle is that the electrolyte needed to fill in all the dead space in the device is in large excess compared to that in pouch cells. This results in uncertainty when studying CEI dissolution in coin cells. Therefore, eventually a pouch cell with targeted capacity, energy, or power is the best platform for cross-validation. The full coin cell protocol listed in Table 1 can quickly identify the most valuable approaches and provides an opportunity for fair comparisons.

Model cathode materials to investigate CEI at high voltages

Cathode stability at high voltages is impacted by both the interfacial and bulk properties of the material. Therefore, a model cathode material that does not undergo significant structural change at high voltages will be critical to explore CEI formation and evolution. One candidate for this is single crystal nickel-rich NMC (NMC=$LiNi_xMn_yCo_zO_2$; $x+y+z\approx1$). For example, single crystal Ni-rich NMC prepared using a molten salt approach (Fig.1a-c) has controlled morphologies that can be used for various purposes. Cylinder-shaped (Fig. 1a) or drum-like NMC76 (Fig. 1b) single crystals expose different facets to the liquid electrolyte, providing a unique opportunity to study the influence of specific lattice plans on CEI formation and decomposition. Single crystal NMC76 can also be grown as large as ~30 μm in diameter (Fig. 1c), and still displays electrochemical activity albeit at a very slow rate (Fig. 1g), making it a perfect platform for *operando* characterization of CEI in a "living" electrochemical cell. Irregularly shaped NMC811 single crystals (Fig. 1d) developed from solid state synthesis [24] provide a good comparison to those formed on crystals grown from molten salts, as the surface properties and impurity levels are quite different. For each model cathode, a baseline performance derived from full coin cells using the corresponding protocols will be critical to benchmark future results.

Commercial polycrystalline NMC811 can also be used as a model. The baseline performance can be used to compare to lab-made cathode materials, using similar cell parameters and testing conditions. Unfortunately, it is not uncommon in the literature to use poorly performing and poorly characterized cathodes as controls to show improvement of modified materials. Figure 2 is an

example of coin cell performance that can be used as a baseline for NMC (or graphite) research. The NMC811 cathode and graphite anode are both from commercial sources. The electrolyte used is the same baseline electrolyte listed in Table 1. Electrodes are constructed corresponding to the key parameters in Table 1. It is clear very stable cycling between 2.6 and 4.2 V is achievable from Graphite/NMC811 coin cells without modifying electrodes or using any additives. Even when the cutoff voltage is increased to 4.3V (vs. graphite), the full coin cell still demonstrated quite stable cycling stability with 82.7% capacity retention after 500 cycles, similar to the one cycled between 2.6 and 4.2V.

In fact, any cathode material can be used as a model material to study the CEI or its own structural stability, as long as the cathode and CEI are the controlling factors determining the cell performance. All the other cell components, such as the anode, SEI, electrolyte, or separator should not be the rate-limiting step or the "weakest" link controlling the overall observed cell behaviors. Once a reliable baseline performance is established, CEI improvements caused by either surface coating or addition of new electrolyte/additive (for example) becomes more distinguishable and reproducible.

Even if certain materials display extraordinary CEI stability at the materials level, using the particles at the electrode level with high mass loading and controlled porosity is still quite challenging.[25,26] For example, while LFP (lithium iron phosphate) has been used in power tools and EVs (electric vehicles), the electrode-level energy density is still limited, in part due to nanostructuring. Dry processing helps to increase the loading and electrode thickness in components containing nanoparticles, with progress in improving rate capabilities of those thick electrodes.[27]

Electrolyte and additives for stabilizing the CEI

High voltage operation of Li-ion batteries: To stabilize the CEI at high voltages, it is necessary to first understand how high is sufficiently high for an EV battery based on Li-ion chemistry. Table 2 compares the gain of capacities and energies and the reduction of cobalt in a 100 kWh EV battery pack adopting Graphite/NMC chemistry charged to various cutoff voltages.

NMC811: The cutoff voltage is usually 4.2 V (vs. graphite, corresponding to 4.3 V vs. Li/Li^+) for commercial Li-ion batteries. If charged to 4.3 V vs. graphite, the usable discharge capacity of NMC811 is increased from 190 mAh/g (at 4.2 V vs. graphite) to 210 mAh/g, accompanied by a slightly increased average discharge voltage. The capacity gain of 20 mAh/g simply by elevating cutoff voltage effectively increases cell level energy and provides more flexibility in cell level design. For the same 100 kWh pack, increasing the cutoff voltage from 4.2 to 4.3V also means less cathode material is needed to meet the energy goal, reducing the pack weight by 17 kg and amount of cobalt by 1kg. Further increasing the cutoff voltage of Gr/NMC811 couple to 4.4 V extracts slightly additional capacity of 5 mAh/g, but the advantages are limited (Table 2). It is probably not worthwhile to increase the upper limit by 100 mV because of the very strict requirements needed for solvent purity and anodic stability. Usually, the entire electrochemical window of the electrolyte shifts towards either higher or lower potentials in the same direction. Expanding the window towards both high and low voltage ends is quite challenging. That means the same electrolyte that stabilizes CEI at very high voltages beyond 4.3 V may become unstable with respect to the anode. Additionally, Ni-rich NMCs are not stable beyond 4.3 V (vs. graphite)

due to phase transitions and increased probability of gas evolution. Therefore, developing a functional electrolyte that ensures a stable CEI above 4.3 V (vs. graphite) may not be useful, unless the structural instability of NMC811 itself is not addressed.

Beyond NMC811: NMC with very high Ni content, e.g., $LiNi_{0.95}Mn_{0.04}Co_{0.01}O_2$ (NMC95) is only stable to 4.04 V vs. graphite[28]. Aggressive side reactions happen between the cathode surface and electrolyte even at 4.18 V (vs. graphite), which is reflected by the continuous cathode impedance growth upon cycling. Therefore, the definition of "high" voltage depends on cathode composition and may differ from that of cells containing NMC-811. Stabilizing Ni-rich NMC below 4.3 V (vs. graphite) or 4.4 V (vs. Li/Li^+) is sufficient to balance energy gain and cycling stability. For example, for $LiNi_{0.9}Mn_{0.05}Co_{0.05}O_2$ (NMC90), the charge cutoff voltage that enables stable cycling may reside between 4.1 and 4.2 V and requires further study. The amount of cobalt in the same 100 kWh EV pack using NMC90 is reduced to half while providing more energy with less battery weight (Table 2). Table 2 also indicates that for NMC90, if the charge cutoff used is 4.2V, the capacity is 195mAh/g, but for a cutoff of 4.3V, 10mAh/g more capacity will be extracted. Even if the electrochemical window is limited to 2.6-4.2V (vs. graphite), the stability of this material is still worse than NMC811 cycled within the same voltage range. This is due to the unstable Ni-rich surface, and increase in impedance upon cycling. Thermal stability is another concern if Ni content is too high in NMC. Single crystal morphologies may help stabilize NMC811 and NMC90 at elevated potentials but more work is still needed. In addition to morphology control, for NMC90 (or compositions with even higher Ni content), stable electrolytes that are resistant to highly active O, suppress cathode impedance growth, and enhance the thermal stability of cathode need to be identified to unlock their full potential. Optimization of Ni content in NMC with a balanced electrochemical window to match currently available functional electrolytes may be a path forward to balancing the energy, cycle life and safety of Li-ion batteries employing high Ni NMCs as the cathodes.

Understand CEI in a battery system

The CEI is the decomposition byproduct of electrolyte on cathode particle surfaces. Therefore, the electrolyte constituents and their relative stability during polarization largely determine the CEI components. The effective evaluation of electrolytes and their derived CEI layers is built upon a few assumptions including but not limited to: (1) the cathode itself is sufficiently good without pre-existing surface impurities left over from synthesis[29] or developed during storage,[19] (2) the electrolyte has no residual water or other impurities that will detrimentally affects the cell performance, and (3) no migration of transition metal cations from cathode to anode, which may damage the SEI causing fast cell degradation. The SEI is always more stable compared to CEI. Some of the modified electrolytes or cathode materials delay the onset voltage for oxidation and gassing in coin cells. Note that the cell impedance is in a reverse relationship with battery dimensions. This means once the same recipe or approach is implemented in realistic batteries, the onset voltages of side reactions will occur earlier than what has been observed in coin cells. In general, the larger the cell format, the earlier onset voltages for gassing if the same electrolyte is used.

Fundamental relationship between inner Helmholtz layer (IHL) and interphase layer formation: Electrochemically, the CEI (or SEI) formation processes are closely related to the components within the electrical double layers **(**Fig. 3) built in the vicinity of the electrode even

before any electrochemical and side reactions start. Before charge transfer happens, anions adsorb on the positively charged cathode surface (left side in Fig.3) along with a small number of solvent molecules, constructing IHL. As the cathode is polarized, these anions will be oxidized and converted to the CEI components. Solvent molecules within the IHL will also be oxidized but unless they have a strong adsorption capability to the cathode or possess very low energy-barrier for oxidation, anions will always be oxidized first within IHL. Therefore, to tune the CEI compositions and properties, addition of certain anions (contributed from Li salts) that will be preferentially oxidized during charge to form an enhanced inorganic layer for CEI may be valuable. If certain solvent additives that are known to help enhance CEI properties will be used in the electrolyte, they need to have a stronger adsorption ability than carbonate solvent molecules in order to fully unlock the potentials of those solvent additives to enhance CEI properties.

Similarly, on the anode side (right side in Fig.3), the electrode is negatively charged. Because Li^+ is surrounded by solvent molecules, most of the chemical species in the IHL of anode are polarized solvent molecules. Some poorly solvated Li^+ and a very small number of anions randomly touch the anode surface as well. Correspondingly, solvent molecules rather than anions play a more important role in tuning SEI properties. This is why without the discovery of the role that EC (ethylene carbonate) plays in forming the SEI, the graphite anode would not have been commercialized successfully. Note that the formation of the CEI and SEI are both correlated to the highest occupied molecular orbital (HOMO) and lowest unoccupied molecular orbital (LUMO) of the electrolyte components, or more directly, the differences of the Gibbs free energy between the reactants (electrolytes) and products after the electrochemical/chemical reactions.[31]

The relationship between IHL and the passivation film formation process also explains why concentrated electrolytes helps formation of good CEI[32] and SEI[33] layers. As the concentration of Li salts increases, anions become more abundant in the IHLs on both the cathode and anode sides enhancing the contribution of anion-derived inorganic components in those passivation films formed on both electrodes.

More evidence can be found in Table 3 which summarizes the functional electrolytes and additives that have been reported in the literature for Ni-rich cathode. Here, we only consider the results for Ni-rich cathodes tested in full coin or pouch cells for the reasons we have discussed earlier.

When the oxidation of Ni-rich materials intensifies at high voltages, conventional carbonates become thermodynamically unstable on their surfaces.[34] EC plays a vital role in forming a stable SEI on graphite but it undergoes significant decomposition concurrently at the cathode side and generates CO_2, CO, and H_2O in the presence of active oxygen released from Ni-rich NMC at elevated potentials.[35] An EC-free electrolyte has been proposed to enhance anodic stability on Ni-rich cathodse by incorporating multiple lithium salts in linear carbonates[36] which in fact tunes the anions within the IHLs of cathode side. Thermodynamically stable solvents, such as sulfones[37], sulfonates[38], nitriles[39], fluorinated carbonates and ethers[3,40-47] are also proposed to enhance CEI properties. However, as discussed earlier, unless those solvents have very strong adsorption ability or have lower oxidation potentials compared to the anions dominantly present in IHL, the impacts from solvent modification on CEI will be limited. More importantly, the change of solvent molecules in the electrolyte affects the SEI more than on CEI because solvents are the dominant species in IHL of anode (Fig.2). While those proposed solvents may or may not enhance the CEI, they will not worsen the SEI, although this needs further investigation. Decoupling the cathode

and anode reactions is critical to understand which component is being impacted more significantly when even a small change is introduced to the cell.[48]

To replace conventional EC-based electrolytes for Li-ion batteries, an overall assessment on the large full cell performances including cycling stability, rate capability, low/high-temperature performance, shelf life, and resistance to abuse, is necessary. At this moment, additives, either solvents or anions, rather than completely switching to a non-carbonate solvent is probably more reasonable for practical applications. Additives that can kinetically form a robust CEI layer on the cathode and prevent further electrolyte decomposition at high voltages are also reported. Many of these additives such as carbon,[49] phosphorus,[50] boron,[51] sulfur,[52]and nitrogen[53] compounds, or their combinations,[54,55] are being developed for cathode materials with relatively low Ni (Ni < 0.8) content, for example NMC442[56,57] or NMC532[58,59] but operating at high voltages of ≥ 4.4 V (vs. graphite). More full cell work is needed to confirm the effectiveness of those previously explored additives for Ni-rich NMC (Ni ≥ 0.8) charged up to 4.4 V (vs. graphite).

While different electrolyte recipes should be developed depending on the specific applications of Li-ion batteries, the unstable nature of Ni-rich surfaces is the root cause that has delayed the large-scale commercialization of high nickel NMC, and therefore needs to be addressed first. In addition to the electrolyte itself, appropriate selection of doping elements or artificial coating layers on cathode may also help to mitigate the electrolyte decomposition and gassing issues commonly found for Ni-rich cathodes.

Integrate characterization and modeling tools to revisit CEI

Characterizing CEI without ambiguity

Since the discovery of CEIs on cathodes in the 1980s[60], there have been many advances in investigating the chemical composition, microstructure, and fine/electronic structure for Li-ion batteries and beyond.

Probing the formation and dynamic evolution of CEI layer structure, chemistry, and properties is extremely challenging due to the sensitive chemical nature, nonuniformity, and complex formation process dependent upon both the cathode active material and liquid electrolyte. The challenges arise not only from the different chemical nature and operating voltages, but also from less controllable factors such as preparation route, porosity, and surface morphology/impurities of cathode materials. For example, the surface native film (LiOH, Li_2CO_3) formed on NMC cathode during synthesis, storage and assembly adds complication to CEI formation and characterization. Model cathode materials with controllable surface properties are critical for CEI investigations with unambiguous results. Flooding of electrolytes will also introduce more interactions between electrolyte, carbon black and binder as well as possible CEI redissolution impeding the investigatation ofthe reactivity of the electrolyte and cathode material, [61,62]

To achieve a holistic understanding of CEI without ambiguity, there is a critical need to develop advanced characterization techniques that are non-destructive, *in-situ/operando* and have high sensitivity, lateral/spatial/temporal resolution, throughput, and automation attributes, and combine these with advanced multiscale modeling tools.

First, due to the sensitive and fragile nature of the CEI, passive and highly sensitive characterization is required to capture its native microstructure and chemistry with minimal damage. For example, transmission electron microscopy (TEM) could provide atomic scale microstructure and chemical information simultaneously, but high energy electron beam and sample preparation via ion milling or ultramicrotomy will contaminate the CEI. Recent advances in cryogenic TEM with nano size cathode particles can reduce damage from the electron beam and TEM sample preparation on the CEI.[63]

Second, validation through the combination of different techniques is essential to obtain more reliable and comprehensive understanding.. For example, the spatial and lateral resolution are both important for the characterization of CEI, but usually challenging to probe simultaneoulsy. Surface sensitive techniques such as X-ray photoelectron spectroscopy (XPS), time-of-flight secondary ion mass spectroscopy (TOF-SIMS) have been used to study the chemical distribution of the CEI with high spectral resolution in large areas, but lack spatial resolution to resolve the nano structural species in CEI. TEM can resolve nanoscopic heterogeneity of the CEI, but the field of view is very small, which raises questions about how representative the localized observation are. [60,64,65]Techniques such as Atomic Force Microscope (AFM) therefore may be used to gain global information on the surface properties of materials or electrodes.

Third, real time monitoring of the CEI dynamic evolution (morphology, composition, and fine structure) is critical to understand its role on the electrochemical performance of a battery.[66] As discussed above in situ/operando methods should be meticulously designed and optimized. This ensures that the information obtained results in information relevant to standard cells.

Fourth, in addition to imaging-based and spectral-based techniques to probe structural and chemical information, the measurement and in-situ monitoring of CEI properties, e.g. ionic conductivity, electrical conductivity, mechanical properties, and thermal properties are also important to understand the relationship between CEI components and properties. For example, the in situ bias TEM technique was recently applied to measure the electronic conductivity of the SEI, and correlated to SEI composition and eventually the electrolyte chemistry.[67] This provides the opportunity to correlate the CEI component and properties, and eventually the battery performance. As discussed above, we also need to carefully design the experiment to build real correlations between CEI and cell performance.

Fifth, current understanding and characterization of the CEI is mainly focused on the laboratory research level (e.g., coin cells), but should be scaled up to 18650 cylindrical cell or pouch cells and eventually packs under realistic cycling conditions, which will benefit industry research as well.[68] Fiber/sensor-based devices integrated into coin cells or pouch cells could be an effective method to monitor chemical, thermal, and molecular level evolution of battery components.[69]

Last, in situ/operando experiments generate huge image and spectral datasets. Properly processing and analyzing data are time-consuming tasks, which can also introduce artifacts. Combining machine learning (ML), artificial intelligence (AI), and advanced characterization techniques could accelerate the data acquisition and analysis with less labor time, human artifacts, high throughput, and automation, which will bring new opportunities for understanding CEI formation and properties.

Providing unbiased interpretations of such experimental results can be nontrivial. For example, many chemical species or local structural motifs that emerge in the CEI present characteristic signals that may differ from those in the bulk. However, this signal disparity may be slight enough that they cannot be easily resolved in many experiments that provide a non-local ensemble averaged measurement of the interface. It is also difficult to elucidate their unique contributions to the CEI formation and function during operation, especially if they are short-lived and fail to be captured by any experimental probes. In this regard, integrating experimental characterization techniques with complementary modeling and simulations at the atomic scale will be highly rewarding as it will help to establish a comprehensive understanding of CEI formation and function.

Challenges and Opportunities in Simulating CEI

Classical molecular dynamics simulations based on empirical representations of interatomic interactions are routinely used to probe interfacial structures and resolve populations of key chemical constituents of the interface. Although this approach may still be time-limited, coupling classical methods with enhanced sampling techniques can enable a more efficient exploration of potential energy surfaces for out-of-equilibrium reactions and processes. The major drawbacks of this approach are the accuracy and transferability of empirical interatomic potentials due to the lack of electronic representation of chemical interactions; these limitations are apparent for even well-parameterized potentials or the more sophisticated class of reactive force fields (ReaxFF). To overcome these challenges, modern machine-learning based force fields that can preserve quantum-level accuracy but at a fraction of the computational cost become increasingly attractive. With the predictive power of molecular dynamics simulations coupled with high-fidelity machine-learning models, it is now possible to survey a wide range of interfacial atomic arrangements and associated reaction pathways and it is becoming increasingly feasible to track interfacial evolution under relevant experimental conditions.

A potential caveat of directly applying atomistic-scale simulations to the study of CEI layers is that any resulting prediction derived from these simulations will exhibit a strong dependence on the quality and complexity of the underlying atomic models. Although this practice presents an opportunity to help isolate and to explore individual factors that contribute to the formation and evolution of the CEI and thus allow the elucidation of structure-property relationships at the interface, it lacks the critical emphasis of realism. Specifically, within this framework, it remains challenging to understand the relevance of key structural and chemical features captured in the model in relation to the materials being used in real electrochemical devices.

Therefore, it is highly desirable to integrate modeling and simulation with solid experimental results and advanced characterization approaches for cross-validation purposes. This concept is illustrated partly in Figure 4. Upon materials selection, baseline measurements can be conducted to inform simulation model, such as composition, exposed crystallographic facets of the cathode, local charge/discharge states, etc. and advise the choice of simulation protocols. Due to the potential complications in modeling open shell transition metal oxides using DFT, special care needs to be taken and comprehensive benchmark tests may become necessary for selecting the appropriate level of theory or DFT exchange-correlation functionals. This is not only critically important to accurately describe the electronic interaction of the cathode material with electrolyte components and thus to predict the propensities for interfacial degradation, but is also essential for

providing reliable training datasets for the development of advanced ML models. Once the ML potentials are successfully trained and validated, large-scale molecular dynamic (MD) simulations with enhanced sampling can be performed to survey the complex interfacial structure, identify kinetically competing reaction pathways, and extract key chemical motifs or representative configurations appeared during interfacial evolution or degradation for spectroscopy calculations. These calculated spectroscopy signatures can be directly used to deconvolute the experimental spectra and provide unbiased elucidation of interfacial sensitivity to external stimuli, such as processing and cell cycling conditions. The comparison with experiment will provide feedback to refine simulation models if necessary to ensure dominate structural and chemical features of interfaces are fully captured. Based on this well implemented experiment-theory feedback loop, a foundational understanding of CEI formation can be established for the model system built and tested using the aforementioned consistent protocol. Positive or negative impacts brought by additives or coating layers used to modify CEI can be analyzed using the same modeling approach to advice design strategies of manipulating the structure and chemistry of CEI to achieve desired performance.

By comparing the theoretical results with experimental measurements collected for samples prepared using different synthetic methods or treated under different conditions, interfacial models can be iteratively revised to ensure essential structural motifs and key chemistry are fully captured. It is only through a well-implemented and well-executed, tightly coupled experiment-simulation approach that a comprehensive atomic-scale description of the dynamically evolving interface can be obtained and its impact on the device-level performance can be elucidated.

Data Availability: All relevant data are included in the paper.

Acknowledgments: This work was supported by the Assistant Secretary for Energy Efficiency and Renewable Energy, Office of Vehicle Technologies of the U.S. Department of Energy (DOE) through Cathode-Electrolyte Interphase (CEI) Consortium. PNNL is operated by Battelle for the Department of Energy under contract DE-AC05-76RLO1830.

Competing interests: The authors declare no competing interests.

Table 1 | Full coin cell parameters in standard testing protocol developed at PNNL.

Cathode: NMC811 (polycrystals or single crystals)	
Active material %	96%
Carbon%	2%
PVDF%	2%
Mass loading (NMC only)	~15 mg/cm^2
Specific capacity	~200 mAh/g (C/10)
Areal Capacity	~ 3 mAh/cm^2
Voltage Window	2.7-4.3V **vs. Gr** (2.8-4.4 V **vs. Li**)
Porosity	~ 35%
Graphite Anode	
Areal Capacity	3.6 mAh/cm^2
Porosity	40-45%
N/P	~1.2
Baseline Electrolyte	1M $LiPF_6$ in EC/EMC(3:7)+2%VC
Formation Cycle	C/10 for charge & discharge for 3 cycles
Charge	CC-CV: C/3 to 4.3V (vs. Gr) then constant voltage until I≤ C/20
Discharge	C/3

Table 2 | Usable capacity and energy from NMC811 charged to different voltages in a 100 kWh Li-ion battery pack.

Material	Voltage Window (V)	Usable Capacity (mAh/g)	Average Discharge Voltage (V)	Material Energy (Wh/kg)	Total NCM mass in 100 kWh LIB pack (kg)	Co Mass (kg)
NMC811	2.7-4.1	180	3.6	648	154	9.3
	2.7-4.2	190	3.65	694	144	8.7
	2.7-4.3	199	3.7	736	136	8.2
	2.7-4.4	204	3.7	759	132	8.0
Material	**Voltage Window (V)**	**Usable Capacity (mAh/g)**	**Average Discharge Voltage (V)**	**Material Energy (Wh/kg)**	**Total NCM mass in 100 kWh LIB pack (kg)**	**Co Mass (kg)**
NMC90	2.7-4.1	185	3.69	683	146	4.4
	2.7-4.2	195	3.73	727	137	4.2
	2.7-4.3	204	3.76	767	130	3.9
	2.7-4.4	212	3.78	803	125	3.8

* Voltage is vs. Graphite; capacity is obtained at C/3 rate.

Table 3 | Functional electrolytes for NMC811 in coin/pouch type lithium-ion batteries using graphite as the anode.

Electrolyte Recipes	Battery Type	Working voltage (V vs. Gr)	Cathode Loading or areal capacity (mg/cm^2 or mAh/cm^2)	Capacity Retention	Charge/ discharge rate	Ref
Based on solvent change or mixing						
$LiPF_6$:MDFA:PFPN:FEC (1:7:0.5:1 by mol)	240 mAh pouch cell	2.8-4.3	13.2	81.8% @ 500 cycles	1C/1C	40
1.0 M $LiPF_6$ PC:TFA (3:7 by vol)	730 mAh pouch cell	2.7-4.3 (45 °C)	12.1	82%@400 cycles	1C/1C	41
1.6 M LiFSI TEOSCN	1 Ah pouch cell	2.8-4.3	N/A	95%@500 cycles	0.2C/ 0.2C	39
1.0 M $LiPF_6$/0.02 M LiDFOB FEC:HFE:FEMC (2:2:6 by vol)	1 Ah pouch cell	3-4.3	N/A (single crystal 811 used)	110.1%@ 200 cycles	0.33C/0.3 3C	42
LiFSI:DMC:EC:TTE (1:4.8:0.2:1 by mol)	Coin cell	2.5-4.4	1.5 mAh/cm^2	69%@ 300 cycles	4C/ 0.33C	3
1.0 M $LiPF_6$ SL:FEC:EMC (1:1:3 by vol) + 0.5wt % $LiBF_4$/$LiNO_3$	Coin cell	2.75-4.4	20	85.2%@ 300 cycles	0.5C/ 0.5C	37
1.0 M $LiPF_6$ in FEC:TTE (6:4 by vol)	1 Ah pouch cell	3-4.4	N/A	91%@ 300 cycles	1C/1C	43
LiFSI:DME:FEC:PFPN (1:1.5:0.5:3 by mol)	coin cell	2.5-4.5	8.35	82%@1000 cycles	0.33C/0.3 3C	44
1.0 M LiTFSI MDFA:MDFSA:TTE (4:1:5 by mol)	Coin cell	2.5-4.5	11.5	80.1%@ 400 cycles	0.5C/ 0.5C	46
0.8 M LiFSI-0.1 M LiTFSI-0.6 M $LiPF_6$ EMC	1 Ah pouch cell	3-4.5	13.5	82.1%@ 200 cycles	0.33C/ 0.33C	36
1.9 M LiFSI TTMS:TM (1:2 by vol)	1 Ah pouch cell	3-4.6	N/A	83%@1000 cycles	0.5C/ 1C	38
LiDFOB:MP:mFT:TTE (1:2.67:1:1 by mol)	1.2 Ah pouch cell	2.8-4.6	17.4	90.4%@ 130 cycles	0.2C/ 0.2C	45
Based on anion change or mixing						
1.0 M $LiPF_6$ EC:EMC (3:7 by wt) + 0.4wt% NaH_2PO_4	Coin cell	3-4.3 (60 °C)	2.6 mAh/cm^2	150 cycles @ 75%, 0.5C/0.5C		50
1.0 M $LiPF_6$ EC:EMC (3:7 by vol) + 2wt% VC	200 mAh pouch cell	2.8-4.4 (40 °C)	N/A	200 cycles @ 80%, 0.2C/0.2C		49
1.0 M $LiPF_6$ EC:EMC (3:7 by vol) + 2wt% VC + 2wt% LiDFOB + 1wt% TMSPi	Coin cell	2.5-4.5	24	300 cycles @ 85%, 0.2C/0.5C		54
1.0 M $LiPF_6$ EC:DEC (1:1 by vol) + 2wt% TMSP+ 0.1 M LiDFOB	Single layer pouch cell	2.7-4.5	N/A	500 cycles @ 82.8%, 1C/1C		55
1.0 M $LiPF_6$ EC:EMC (1:2 by vol) + 1wt% DES	1.95 Ah pouch cell	2.75-4.5	N/A	150 cycles @ 82.5%, 1C/1C		52

Abbreviation:

Methyl difluoroacetate (MDFA); Ethoxy-pentafluoro-cyclotriphosphazene (PFPN); Fluoroethylene carbonate (FEC); Propylene carbonate (PC); 2,2,2-trifluoroethyl acetate (TFA); (2-cyanoethyl)triethoxysilane (TEOSCN); (2,2,2-trifluoroethyl) carbonate (FEMC); Dimethyl carbonate (DMC); Ethylene carbonate (EC); 1,1,2,2-tetrafluoroethyl-2,2,3,3-tetrafluoropropyl ether (TTE); Sulfolane (SL); Ethyl methyl carbonate (EMC); Ethoxy(pentafluoro) cyclotriphosphazene (PFPN); Dimethoxyethane (DME); Methyl difluoroacetate (MDFA); Methyl 2,2-difluoro-2 (fluorosulfonyl)acetate (MDFSA); 2,2,2-trifluoroethyl trifluoromethanesulfonate (TTMS); 2,2,2-trifluoroethyl methanesulfonate (TM); Methyl propionate (MP); m-fluorotoluene (mFT); Vinylene carbonate (VC); Tris(trimethylsilyl)phosphite (TMSPi); Diethyl carbonate (DEC); Tris(trimethylsilyl)phosphate(TMSP); 3,3-Diethylene Di-Sulfite (DES); 2,2,7,7-tetramethyl-3,6-dioxa-2,7-disilaoctane-4,4,5,5-tetracarbonitrile (TDSTCN).

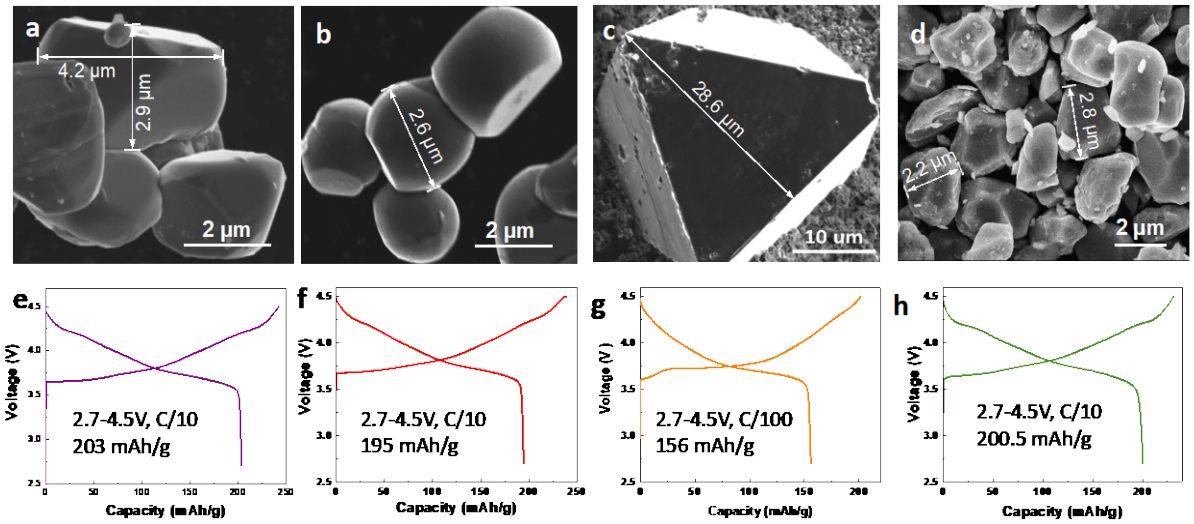

Fig. 1 | Single crystal Ni-rich NMC with different morphologies as model materials. **a**, single crystal NMC76 with an average crystal size of 3-4 μm. **b**, modified single crystal NMC76 with drum-like morphologies. **c**, ca. 20 μm large single crystal NMC76 with (001) and (012) planes exposed, ideal for in situ characterizations. **d**, Single crystal NMC811 with irregular morphologies. **e**, The charge-discharge curve of single crystal NMC76 in **a**. 203 mAh/g capacity is delivered when charged to 4.5 V vs. Li/Li^+. **f**, The charge-discharge curve of drum-like single crystals in **b**. 195 mAh/g capacity is delivered when charged to 4.5 V vs. Li/Li^+. **g**, The charge-discharge curve of 20 μm single crystal in **c**. At a very slow rate of C/100, still 156 mAh/g capacity is delivered from such as huge crystal when charged to 4.5 V vs. Li/Li^+. **h**, The charge-discharge curve of ca. 2 μm single crystal in **d**. 202 mAh/g capacity is obtained when charged to 4.4 V vs. Li/Li^+. **a-c** are synthesized by a molten salt approach as published in reference[70], while **d** prepared by using solid state synthesis[71].

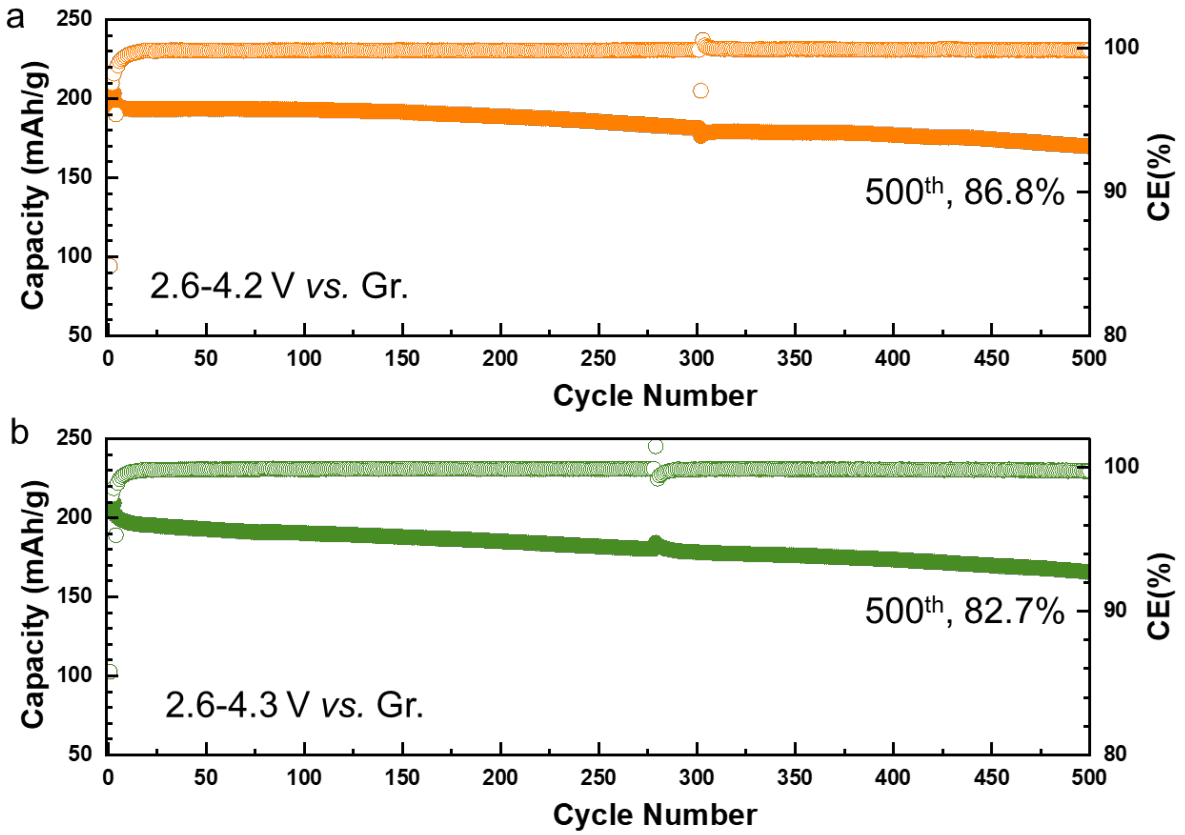

Fig. 2 | Electrochemical performances of NMC811 polycrystals tested in full coin cells which use graphite as anode. **a**, Cycling performance of NMC811 tested between 2.6-4.2V vs. Gr. **b**, Cycling performance of NMC811 tested between 2.6-4.3V vs. Gr. Commercial NMC811 cathode and graphite anode materials are used in this full coin cell testing by using the protocols listed in Table 1. Baseline electrolyte. i.e., 1M $LiPF_6$ in EC/EMC+2%VC, is used for coin cell testing. C/3 was used for both charge and discharge after three formation cycles at C/10. 1C was named as 200 mA/g. These performances can be used as baseline performances to benchmark any further modification in cathode, anode or electrolyte etc.

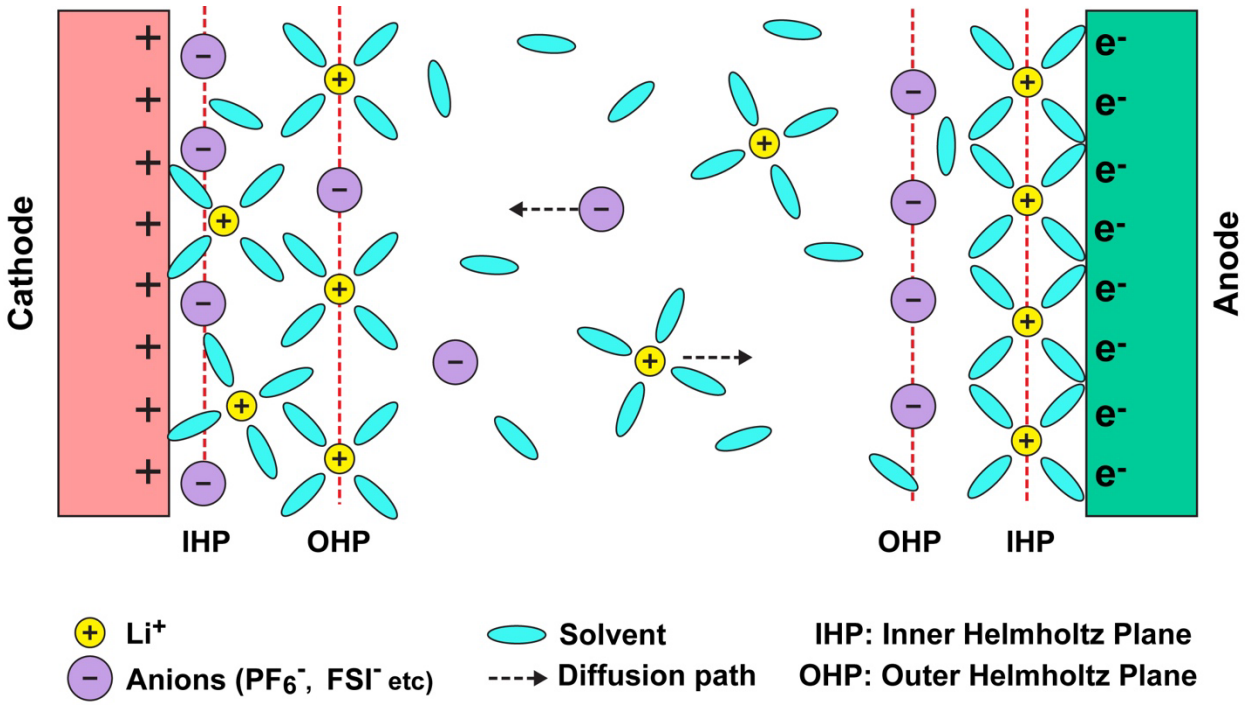

Fig. 3 | Electrical double layers formed on cathode and anode sides. The constituents in the inner Helmholtz layer are related to the later formed passion layers on cathode and anodes, which can be used to help develop better electrolytes or additives to tune CEI or SEI properties.

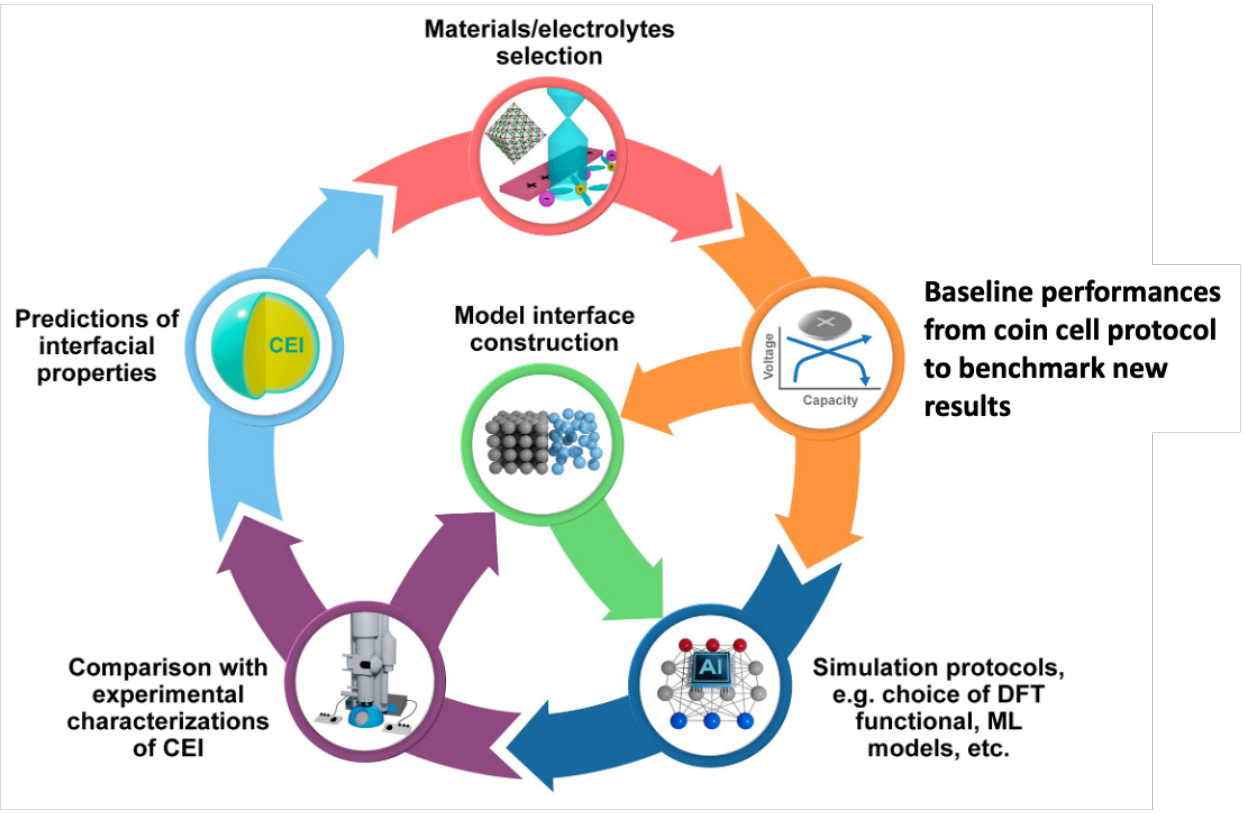

Fig. 4 | An approach for resolving the chemical and structural features of complex electrochemical interfaces based on the integration of experiments and theory. Libraries of local interfacial structures and their associated chemical and structural signatures are constructed and compared against experimentally-measured signatures in order to iteratively refine structural and chemical models.

References

1 Xu, K. Electrolytes and interphases in Li-ion batteries and beyond. *Chem. Rev.* **114**, 11503-11618 (2014).

2 Ohzuku, T., Iwakoshi, Y. & Sawai, K. Formation of lithium-graphite intercalation compounds in nonaqueous electrolytes and their application as a negative electrode for a lithium ion (shuttlecock) cell. *J. Electrochem. Soc.* **140**, 2490 (1993).

3 Kautz, D. J. et al. Designing electrolytes with controlled solvation structure for fast-charging lithium-ion batteries. *Adv. Energy Mater.* **13**, 2301199 (2023).

4 Zhang, X. et al. Advanced electrolytes for fast-charging high-voltage lithium-ion batteries in wide-temperature range. *Adv. Energy Mater.* **10**, 2000368 (2020).

5 Wen, B. et al. Ultrafast ion transport at a cathode–electrolyte interface and its strong dependence on salt solvation. *Nat. Energy* **5**, 578-586 (2020).

6 Björklund, E. et al. Cycle-induced interfacial degradation and transition-metal cross-over in $LiNi_{0.8}Mn_{0.1}Co_{0.1}O_2$–graphite cells. *Chem. Mater.* **34**, 2034-2048 (2022).

7 Liu, W. et al. Inhibition of transition metals dissolution in cobalt-free cathode with ultrathin robust interphase in concentrated electrolyte. *Nat. Commun.* **11**, 3629 (2020).

8 Gutierrez, A. et al. Review—Earth-abundant, Mn-rich cathodes for vehicle applications and beyond: Overview of critical barriers. *J. Electrochem. Soc.* **170**, 030509 (2023).

9 Clément, R. J., Lun, Z. & Ceder, G. Cation-disordered rocksalt transition metal oxides and oxyfluorides for high energy lithium-ion cathodes. *Energy Environ. Sci.* **13**, 345-373 (2020).

10 Nelson, K. J. et al. Studies of the effect of high voltage on the impedance and cycling performance of $Li[Ni_{0.4}Mn_{0.4}Co_{0.2}]O_2$/graphite lithium-ion pouch cells. *J. Electrochem. Soc.* **162**, A1046-A1054 (2015).

11 Yan, P. et al. Tailoring grain boundary structures and chemistry of Ni-rich layered cathodes for enhanced cycle stability of lithium-ion batteries. *Nat. Energy* **3**, 600-605 (2018).

12 Hu, J. et al. Locking oxygen in lattice: A quantifiable comparison of gas generation in polycrystalline and single crystal Ni-rich cathodes. *Energy Storage Mater.* **47**, 195-202 (2022).

13 Bi, Y. et al. Reversible planar gliding and microcracking in a single-crystalline Ni-rich cathode. *Science* **370**, 1313-1317 (2020).

14 Lin, F. et al. Metal segregation in hierarchically structured cathode materials for high-energy lithium batteries. *Nat. Energy* **1**, 15004 (2016).

15 Yan, P. et al. Ni and Co segregations on selective surface facets and rational design of layered lithium transition-metal oxide cathodes. *Adv. Energy Mater.* **6**, 1502455 (2016).

16 Zhang, J. et al. Interfacial design for a 4.6 V high-voltage single-crystalline $LiCoO_2$ cathode. *Adv. Mater.* **34**, 2108353 (2022).

17 Choi, S. H., Son, J.-W., Yoon, Y. S. & Kim, J. Particle size effects on temperature-dependent performance of $LiCoO_2$ in lithium batteries. *J. Power Sources* **158**, 1419-1424 (2006).

18 Zhang, X. et al. Electrolyte regulating toward stabilization of cobalt-free ultrahigh-nickel layered oxide cathode in lithium-ion batteries. *ACS Energy Lett.* **6**, 1324-1332 (2021).

19 Jung, R. et al. Effect of ambient storage on the degradation of ni-rich positive electrode materials (NMC811) for Li-ion batteries. *J. Electrochem. Soc.* **165**, A132-A141 (2018).

20 Liu, D. et al. Review of recent development of in situ/operando characterization techniques for lithium battery research. *Adv. Mater.* **31**, 1806620 (2019).

21 Chen, S. et al. Critical parameters for evaluating coin cells and pouch cells of rechargeable Li-metal batteries. *Joule* **3**, 1094-1105 (2019).

22 Xiao, J. et al. Perspective—Electrochemistry in understanding and designing electrochemical energy storage systems. *J. Electrochem. Soc.* **169**, 010524 (2022).
23 Hu, J. et al. Achieving highly reproducible results in graphite-based Li-ion full coin cells. *Joule* **5**, 1011-1015 (2021).
24 Bi, Y. et al. Highly stable Ni-rich layered oxide cathode enabled by a thick protective layer with bio-tissue structure. *Energy Storage Mater.* **24**, 291-296 (2020).
25 Lu, D. et al. Enabling high-energy-density cathode for lithium–sulfur batteries. *ACS Appl. Mater. Interfaces* **10**, 23094-23102 (2018).
26 Xiao, J. Understanding the lithium sulfur battery system at relevant scales. *Adv. Energy Mater.* **5**, 1501102 (2015).
27 Chouchane, M., Yao, W., Cronk, A., Zhang, M. & Meng, Y. S. Improved rate capability for dry thick electrodes through finite elements method and machine learning coupling. *ACS Energy Lett.* 1480-1486 (2024).
28 Zhang, N. et al. Long-term cycling and mechanisms of cell degradation of single crystal $LiNi_{0.95}Mn_{0.04}Co_{0.01}O_2$/graphite cells. *J. Electrochem. Soc.* **171**, 010520 (2024).
29 Bi, Y., Li, Q., Yi, R. & Xiao, J. To pave the way for large-scale electrode processing of moisture-sensitive Ni-rich cathodes. *J. Electrochem. Soc.* **169**, 020521 (2022).
30 Cao, X. Important factors for the reliable and reproducible preparation of non-aqueous electrolyte solutions for lithium batteries. *Commun. Mater.* **4**, 10 (2023).
31 Peljo, P. & Girault, H. H. Electrochemical potential window of battery electrolytes: the HOMO–LUMO misconception. *Energy Environ. Sci.* **11**, 2306-2309 (2018).
32 Cao, X. et al. Optimization of fluorinated orthoformate based electrolytes for practical high-voltage lithium metal batteries. *Energy Storage Mater.* **34**, 76-84 (2021).
33 Yamada, Y. et al. Unusual stability of acetonitrile-based superconcentrated electrolytes for fast-charging lithium-ion batteries. *J. Am. Chem. Soc.* **136**, 5039-5046 (2014).
34 Dong, T. et al. Electrolyte engineering toward high performance high nickel (Ni ≥ 80%) lithium-ion batteries. *Adv. Sci.* **11**, 2305753 (2023).
35 Rinkel, B. L. D., Vivek, J. P., Garcia-Araez, N. & Grey, C. P. Two electrolyte decomposition pathways at nickel-rich cathode surfaces in lithium-ion batteries. *Energy Environ. Sci.* **15**, 3416-3438 (2022).
36 Wu, Y. et al. High-voltage and high-safety practical lithium batteries with ethylene carbonate-free electrolyte. *Adv. Energy Mater.* **11**, 2102299 (2021).
37 Dai, P. et al. Synergistic effect of dual-anion additives promotes the fast dynamics and high-voltage performance of Ni-rich lithium-ion batteries by regulating the electrode/electrolyte interface. *ACS Applied Mater. Interfaces* **14**, 39927-39938 (2022).
38 Zhang, J. et al. Multifunctional solvent molecule design enables high-voltage Li-ion batteries. *Nat. Commun.* **14**, 2211 (2023).
39 Lu, D. et al. A self-purifying electrolyte enables high energy Li ion batteries. *Energy Environ. Sci.* **15**, 3331-3342 (2022).
40 Zou, Y. et al. Non-flammable electrolyte enables high-voltage and wide-temperature lithium-ion batteries with fast charging. *Angew. Chem. Int. Ed.* **62**, e202216189 (2023).
41 An, K., Tran, Y. H. T., Kwak, S., Han, J. & Song, S.-W. Design of fire-resistant liquid electrolyte formulation for safe and long-cycled lithium-ion batteries. *Adv. Funct. Mater.* **31**, 2106102 (2021).
42 Wu, C. et al. Thermal runaway suppression of high-energy lithium-ion batteries by designing the stable interphase. *J. Electrochem. Soc.* **168**, 090563 (2021).

43 Hou, J. et al. Thermal runaway of lithium-ion batteries employing flame-retardant fluorinated electrolytes. *Energy Environ. Mater.* **6**, e12297 (2023).
44 Chen, L. et al. High-safety and high-efficiency electrolyte design for 4.6 V-class lithium-ion batteries with a non-solvating flame-retardant. *Chem. Sci.* **14**, 1184-1193 (2023).
45 Fang, M. et al. An electrolyte with less space-occupying diluent at cathode inner helmholtz plane for stable 4.6 V lithium-ion batteries. *Angew. Chem. Int. Ed.* **63**, e202316839 (2023).
46 Xu, J. et al. Electrolyte design for Li-ion batteries under extreme operating conditions. *Nature* **614**, (2023).
47 Jia, H. et al. Toward the practical use of cobalt-free lithium-ion batteries by an advanced ether-based electrolyte. *ACS Appl. Mater. Interfaces* **13**, 44339-44347 (2021).
48 Páez Fajardo, G. J. et al. Synergistic degradation mechanism in single crystal Ni-rich NMC//graphite cells. *ACS Energy Lett.* **8**, 5025-5031 (2023).
49 Li, J., Downie, L. E., Ma, L., Qiu, W. & Dahn, J. R. Study of the failure mechanisms of $LiNi_{0.8}Mn_{0.1}Co_{0.1}O_2$ cathode material for lithium ion batteries. *J. Electrochem. Soc.* **162**, A1401-A1408 (2015).
50 Jo, M., Park, S.-H. & Lee, H. NaH_2PO_4 as an electrolyte additive for enhanced thermal stability of $LiNi_{0.8}Co_{0.1}Mn_{0.1}O_2$/graphite batteries. *J. Electrochem. Soc.* **167**, 130502 (2020).
51 Li, J., Li, W., You, Y. & Manthiram, A. Extending the service life of high-Ni layered oxides by tuning the electrode–electrolyte interphase. *Adv. Energy Mater.* **8**, 1801957 (2018).
52 Li, S. et al. 3,3-diethylene di-sulfite (DES) as a high-voltage electrolyte additive for 4.5 V $LiNi_{0.8}Co_{0.1}Mn_{0.1}O_2$/graphite batteries with enhanced performances. *ChemElectroChem* **8**, 745-754 (2021).
53 Ren, Z. et al. Delicately designed cyano-siloxane as multifunctional additive enabling high voltage $LiNi_{0.9}Co_{0.05}Mn_{0.05}O_2$/graphite full cell with long cycle life at 50 °C. *Adv. Funct. Mater.* **33**, 2302411 (2023).
54 Zhao, W. et al. Extending the high-voltage operation of graphite/NCM811 cells by constructing a robust electrode/electrolyte interphase layer. *Mater. Today Energy* **34**, 101301 (2023).
55 Cheng, F. et al. Tailoring electrolyte enables high-voltage Ni-rich NCM cathode against aggressive cathode chemistries for Li-ion batteries. *Sci. Bull.* **67**, 2225-2234 (2022).
56 Ma, L., Xia, J. & Dahn, J. R. Improving the high voltage cycling of $Li[Ni_{0.42}Mn_{0.42}Co_{0.16}]O_2$ (NMC442)/graphite pouch cells using electrolyte additives. *J. Electrochem. Soc.* **161**, A2250-A2254 (2014).
57 Xia, J. et al. Study of triallyl phosphate as an electrolyte additive for high voltage lithium-ion cells. *J. Power Sources* **295**, 203-211 (2015).
58 Keefe, A. S., Weber, R., Hill, I. G. & Dahn, J. R. Studies of the SEI layers in $Li(Ni_{0.5}Mn_{0.3}Co_{0.2})O_2$/artificial graphite cells after formation and after cycling. *J. Electrochem. Soc.* **167**, 120507 (2020).
59 Thompson, L. M. et al. Quantifying changes to the electrolyte and negative electrode in aged NMC532/graphite lithium-ion cells. *J. Electrochem. Soc.* **165**, A2732-A2740 (2018).
60 Thomas, M. G. S. R., Bruce, P. G. & Goodenough, J. B. AC impedance analysis of polycrystalline insertion electrodes - application to $Li_{1-x}CoO_2$. *J. Electrochem. Soc.* **132**, 1521-1528. (1985).
61 Demeaux, J., Caillon-Caravanier, M., Galiano, H., Lemordant, D. & Claude-Montigny, B. LiNiMnO/electrolyte and carbon black/electrolyte high voltage interfaces: To evidence the

chemical and electronic contributions of the solvent on the cathode-electrolyte interface formation. *J. Electrochem. Soc.* **159**, A1880-A1890 (2012).
62 Gauthier, M. et al. Electrode-electrolyte interface in li-ion batteries: Current understanding and new insights. *J. Phys. Chem. Lett.* **6**, 4653-4672 (2015).
63 Zhang, Z. W. et al. Cathode-electrolyte interphase in lithium batteries revealed by cryogenic electron microscopy. *Matter* **4**, 302-312 (2021).
64 Huang, W., Wang, H., Boyle, D. T., Li, Y. Z. & Cui, Y. Resolving nanoscopic and mesoscopic heterogeneity of fluorinated species in battery solid-electrolyte interphases by cryogenic electron microscopy. *ACS Energy Lett.* **5**, 1128-1135 (2020).
65 Hestenes, J. C. & Marbella, L. E. Beyond composition: Surface reactivity and structural arrangement of the cathode-electrolyte interphase. *ACS Energy Lett.* **8**, 4572-4596 (2023).
66 Lu, J., Wu, T. P. & Amine, K. State-of-the-art characterization techniques for advanced lithium-ion batteries. *Nat. Energy* **2**, 17011 (2017).
67 Xu, Y. et al. Direct in situ measurements of electrical properties of solid–electrolyte interphase on lithium metal anodes. *Nat. Energy* **8**, 1345-1354 (2023).
68 Xiao, J., Shi, F. F., Glossmann, T., Burnett, C. & Liu, Z. From laboratory innovations to materials manufacturing for lithium-based batteries. *Nat. Energy* **8**, 329-339 (2023).
69 Huang, J. Q., Boles, S. T. & Tarascon, J. M. Sensing as the key to battery lifetime and sustainability. *Nat. Sustain.* **5**, 194-204 (2022).
70 Moiseev, I. A. et al. Single crystal Ni-rich NMC cathode materials for lithium-ion batteries with ultra-high volumetric energy density. *Energy Adv.* **1**, 677-681 (2022).
71 Bi, Y. et al. Simultaneous single crystal growth and segregation of Ni-rich cathode enabled by nanoscale phase separation for advanced lithium-ion batteries. *Energy Storage Mater.* **62**, 102947 (2023).